THE JOURNAL OF BIOLOGICAL CHEMISTRY VOL. 289, NO. 34, pp. 23977–23991, August 22, 2014
Published in the U.S.A.

Magnesium Modulates Actin Binding and ADP Release in Myosin Motors*

Received for publication, March 5, 2014, and in revised form, July 7, 2014 Published, JBC Papers in Press, July 8, 2014, DOI 10.1074/jbc.M114.562231

Anja M. Swenson[‡], Darshan V. Trivedi[‡], Anna A. Rauscher[§], Yuan Wang[¶], Yasuharu Takagi[‖], Bradley M. Palmer[¶], András Málnási-Csizmadia[§], Edward P. Debold[‡‡], and Christopher M. Yengo[‡1]**

*From the [‡]Department of Cellular and Molecular Physiology, Pennsylvania State University College of Medicine, Hershey, Pennsylvania 17033, the [§]Department of Biochemistry, Eötvös Loránd University, H-1117 Budapest, Hungary, the [¶]Department of Molecular Physiology and Biophysics, University of Vermont, Burlington, Vermont 05405, the [‖]Laboratory of Molecular Physiology, NHLBI, National Institutes of Health, Bethesda, Maryland 20892, the [‡‡]Department of Kinesiology, University of Massachusetts, Amherst, Massachusetts 02210, and the **Hungarian Academy of Sciences-Eötvös Loránd University Molecular Biophysics Research Group, H-1117 Budapest, Hungary*

Background: Magnesium may be an important physiological regulator of myosin motor activity.
Results: Mg^{2+} inhibits the ADP release rate constant in the subset of myosins examined and reduces actin affinity in the post-hydrolysis state in myosin V.
Conclusion: Mg^{2+} alters contractile velocity without altering overall tension-generating capacity.
Significance: Mg^{2+}-dependent regulation of motor activity is conserved in myosin motors.

We examined the magnesium dependence of five class II myosins, including fast skeletal muscle myosin, smooth muscle myosin, β-cardiac myosin (CMIIB), *Dictyostelium* myosin II (DdMII), and nonmuscle myosin IIA, as well as myosin V. We found that the myosins examined are inhibited in a Mg^{2+}-dependent manner (0.3–9.0 mM free Mg^{2+}) in both ATPase and motility assays, under conditions in which the ionic strength was held constant. We found that the ADP release rate constant is reduced by Mg^{2+} in myosin V, smooth muscle myosin, nonmuscle myosin IIA, CMIIB, and DdMII, although the ADP affinity is fairly insensitive to Mg^{2+} in fast skeletal muscle myosin, CMIIB, and DdMII. Single tryptophan probes in the switch I (Trp-239) and switch II (Trp-501) region of DdMII demonstrate these conserved regions of the active site are sensitive to Mg^{2+} coordination. Cardiac muscle fiber mechanic studies demonstrate cross-bridge attachment time is increased at higher Mg^{2+} concentrations, demonstrating that the ADP release rate constant is slowed by Mg^{2+} in the context of an activated muscle fiber. Direct measurements of phosphate release in myosin V demonstrate that Mg^{2+} reduces actin affinity in the M·ADP·P_i state, although it does not change the rate of phosphate release. Therefore, the Mg^{2+} inhibition of the actin-activated ATPase activity observed in class II myosins is likely the result of Mg^{2+}-dependent alterations in actin binding. Overall, our results suggest that Mg^{2+} reduces the ADP release rate constant and rate of attachment to actin in both high and low duty ratio myosins.

Magnesium is an abundant divalent cation known for its role as an essential metal cofactor for many enzymes that utilize nucleotide triphosphates (NTPs) as an intracellular energy source. Previous studies with motor proteins such as myosin traditionally focus on the role of Mg^{2+} as a cofactor in ATP binding, hydrolysis, and product release in the force-generating mechanochemical cycle (1, 2). Recent studies highlight the possibility that free Mg^{2+} can modulate motor activity and thus physiological function in muscle myosin II and unconventional myosins I, V, and VII (3–7). These studies generally support a mechanism whereby Mg^{2+} alters key steps in the mechanochemical cycle, including the ADP release rate constant, which is an important determinant of duty ratio (fraction of the ATPase cycle myosin remains attached to actin). However, it remains unclear to what degree other steps of the actomyosin ATPase cycle are impacted by Mg^{2+}. In addition, it is unclear if Mg^{2+}-dependent modulation of myosin motor activity is conserved throughout the myosin superfamily.

Several NTPase superfamilies, including myosins, kinesins, and G proteins, share highly conserved elements in their nucleotide binding regions (8). The P-loop, switch I, and switch II are involved in NTP binding, hydrolysis, and Mg^{2+} coordination. In myosins, these conserved elements have the ability to amplify small changes in the nucleotide binding region to large scale force-generating movements of the light chain binding region or lever arm. Our previous work has focused on the impact of Mg^{2+} on myosin V (MV),[2] a ubiquitous intracellular transporter that has been well characterized both structurally and biochemically (9). Studies in myosin V have supported a strain-sensitive two-state model for ADP release (10–12). Myosin binding to actin in the post-hydrolysis ADP·P_i state (K_9) results in acceleration of phosphate release (k'_{+4}) and forma-

* This work was supported, in whole or in part, by National Institutes of Health Grant R01 EY016419 and Grant R01 HL086902 (to B. M. P.). This work was also supported by a grant from the Pennsylvania Department of Health (to C. M. Y.), National Science Foundation Grant EPS-1101317, and European Research Council Ideas 208319 (to A. M. C.).

[1] To whom correspondence should be addressed: Dept. of Cellular and Molecular Physiology, Pennsylvania State University College of Medicine, 500 University Dr., Hershey, PA 17033. Tel.: 717-531-8575; E-mail: cyengo@hmc.psu.edu.

[2] The abbreviations used are: MV, myosin V; SKII, fast skeletal muscle myosin; SMII, smooth muscle myosin; CMIIB, β-cardiac myosin; DdMII, *Dictyostelium* myosin II; NMIIA, nonmuscle myosin IIA; mant-dADP, *N*-methylanthraniloyl (mant)-labeled 2′-deoxy-ADP.

$$\begin{array}{ccccccccc} \mathrm{AM}+\mathrm{ATP} & \overset{K'_1K'_2}{\leftrightarrow} & \mathbf{AM.ATP} & \overset{K'_3}{\leftrightarrow} & \mathbf{AM.ADP.Pi} & \overset{K'_4}{\leftrightarrow} & \mathrm{AM^*.ADP} & \overset{K'_{5A}}{\leftrightarrow} \mathrm{AM.ADP} & \overset{K'_{5B}}{\leftrightarrow} \mathrm{AM} \\ \uparrow\downarrow K_6 & & \uparrow\downarrow K_8 & & \uparrow\downarrow K_9 & & \uparrow\downarrow K_{10A} & & \uparrow\downarrow K_{10B} \quad \uparrow\downarrow K_6 \\ \mathrm{M}+\mathrm{ATP} & \overset{K_1K_2}{\leftrightarrow} & \mathbf{M.ATP} & \overset{K_3}{\leftrightarrow} & \mathbf{M.ADP.Pi} & \overset{K_4}{\leftrightarrow} & \mathrm{M^*.ADP} & \overset{K_{5A}}{\leftrightarrow} \mathrm{M.ADP} & \overset{K_{5B}}{\leftrightarrow} \mathrm{M} \end{array}$$

Scheme 1.

tion of the actomyosin·ADP state with a high affinity for ADP (Scheme 1). An active site isomerization results in a weakening of the affinity for ADP (k'_{+5A}) and promotes the release of nucleotide (k'_{+5B}). In the presence of actin, Mg^{2+} is thought to exchange readily from both actomyosin·ADP states and can alter both the transition between actomyosin·ADP states and the release of ADP (5, 6, 9). Because the ADP release step is rate-limiting in myosin V, increasing free Mg^{2+} concentration slows the myosin V ATPase activity as well as sliding velocity (9, 13) based on a detachment-limited model for *in vitro* motility. The detachment-limited model (14) suggests that sliding velocity (V) is inversely proportional to the attached time (t_{on}), the period of time myosin is strongly attached to actin, and is proportional to the size of the unitary displacement (d_{uni}), the displacement generated by a single myosin motor (Equation 1).

$$V = d_{uni}/t_{on} \qquad \text{(Eq. 1)}$$

Therefore, the Mg^{2+} dependence of *in vitro* sliding velocity should correlate with the Mg^{2+} dependence of the ADP release rate constant in myosins that follow a detachment-limited model.

Recent studies in other unconventional myosins support a conserved mechanism for Mg^{2+} inhibition of the ADP release steps. In addition, these studies suggest that Mg^{2+} can facilitate the transition between a motor that is a transporter or a tension generator (7). For example, regulation of myosin I occurs at Mg^{2+} concentrations between 0.3 and 1 mM free Mg^{2+}, which is within the concentration range measured intracellularly (4). A study on myosin VII, a mechanoenzyme involved in auditory and visual processes, reveals a similar sub-millimolar Mg^{2+} sensitivity with total inhibition of sliding velocity above 1 mM free Mg^{2+} (7). Although intracellular Mg^{2+} concentrations are traditionally thought to be maintained within a narrow range, recent studies are challenging this view with the report of large Mg^{2+} gradients in the cell (15). In muscle, the free Mg^{2+} concentration ranges from 0.7 mM in cardiac muscle (16) to 0.9–1.3 mM in skeletal muscle (17, 18). In addition, alterations in free Mg^{2+} concentrations have been associated with cardiovascular disease (19) and contractile performance (20). Taken together, these findings highlight the importance of investigating the conserved mechanisms of Mg^{2+}-dependent modulation of myosin motor activity.

Structural and biochemical studies of *Dictyostelium* myosin II have contributed significantly to an enhanced understanding of the mechanochemical cycle of class II myosins (21). A study on *Dictyostelium* myosin II is in general agreement with myosin V studies regarding the presence of two actomyosin ADP states (3). However, this work proposed that Mg^{2+} exchanges from the weak actomyosin·ADP state exclusively, which could potentially be the result of class-specific variations in Mg^{2+} coordination. One residue in the switch II region of myosin V (Tyr-439 in myosin V, which corresponds to Ser-456 in *Dictyostelium*) was studied by Nagy *et al.* (22) and proposed to be an important mediator of Mg^{2+} binding affinity. Variability at this conserved residue may be one contributing factor for the increased sensitivity to Mg^{2+} observed in some unconventional myosins.

In this study, we directly compare the impact of Mg^{2+} on a subset of muscle and nonmuscle myosins. We find the major impact of Mg^{2+} manifests itself differently based on characteristic rate-limiting step differences in myosins. Our results support a model in which increasing Mg^{2+} concentration universally slows actomyosin ATPase activity, *in vitro* actin sliding, and contractile velocity in muscle in a manner independent of ionic strength. We demonstrate that multiple steps in the actomyosin ATPase cycle are sensitive to changes in physiological free Mg^{2+} concentrations.

EXPERIMENTAL PROCEDURES

Reagents and Actin Preparation—All reagents were of the highest quality and purity commercially obtainable. ATP and ADP were prepared fresh from powder, and the concentrations were measured by absorbance at 259 nm with ϵ_{259} = 15,400 $M^{-1}-cm^{-1}$ (23). *N*-Methylanthraniloyl (mant)-labeled 2′-deoxy-ADP (mant-dADP) was purchased from Jena Scientific. The mant-dADP concentration was determined by absorbance at 255 nm and ϵ_{255} = 23,300 $M^{-1}\cdot cm^{-1}$.

Protein Expression and Purification—The baculovirus/SF9 cell system was used to co-express a heavy meromyosin (HMM) version of *Gallus gallus* myosin VA containing an N-terminal FLAG tag and C-terminal YFP (MV) with calmodulin (24). A version of myosin VA containing a single IQ motif and C-terminal Myc and FLAG tags was co-expressed with calmodulin as described (25). The *G. gallus* smooth muscle myosin HMM with a C-terminal FLAG and Myc tag (SMII) (26) and *Mus musculus* nonmuscle myosin IIA HMM with a C-terminal FLAG tag (NMIIA) (27) were co-expressed with their associated light chains. All baculovirus/SF9 cell expressed constructs were purified by anti-FLAG affinity chromatography (24–27). The single tryptophan containing (Trp-239 and Trp-501) *Dictyostelium* myosin II motor domain (DdMII) constructs was prepared as described (3, 28). Rabbit psoas skeletal muscle was used to prepare skeletal muscle myosin HMM (SKII) (29). β-Cardiac HMM (CMIIB) was purified from pig hearts as described (29) with modification (30). Prior to characterization, SMII and NMIIA were phosphorylated with myosin light chain kinase (27). Rabbit smooth muscle light chain kinase was expressed in Sf9 cells, purified by anti-FLAG affinity chromatography, and stored at −80 °C (24, 26). An actin spin-down assay was performed on tissue-purified SKII and CMIIB prior to analysis to maximize the ratio of active to nonactive myosin heads. *G. gallus* calmodulin was expressed and purified as described (31). Myosin concentrations were determined by absorbance at 280 nm (MV 1IQ, ϵ_{280} = 103,600 $M^{-1}\cdot cm^{-1}$, SKII, ϵ_{280} = 210,000 $M^{-1}\cdot cm^{-1}$) or by Bio-Rad microplate assay using bovine serum albumin (BSA) as a standard. Actin was prepared from rabbit skeletal muscle using the acetone powder method (32). Pyrene-labeled actin was prepared with *N*-(1-pyrene)iodoacetamide (Invitrogen) as described (33).

Buffer Conditions—MV experiments were performed in KMg50 buffer (10 mM imidazole, 50 mM KCl, 1 mM EGTA, 0.5 mM $MgCl_2$, 1 mM DTT, pH 7.0, 25 °C). Myosin II experiments were carried out in a lower ionic strength MOPS buffer (10 or 20 mM KCl, 20 mM MOPS, 1 mM EGTA, 0.5 mM $MgCl_2$, 1 mM DTT, pH 7.0, 25 °C). A constant ionic strength of 0.05 M for myosin II (except actin-activated ATPase experiments, Fig. 1, in which 0.04 M was used) and 0.08 M for myosin V was maintained throughout all assays by varying KCl concentrations to balance changes in $MgCl_2$ concentration. The buffer used for DdMII experiments was 20 mM HEPES, pH 7.3, whereas $MgCl_2$ concentrations were varied, and ionic strength was compensated by changing NaCl concentrations (*i.e.* 120 mM NaCl, 0 mM $MgCl_2$ or 60 mM $NaCl_2$, 20 mM $MgCl_2$). Free Mg^{2+} concentrations were calculated using MaxC 2.5.

Stopped-flow Kinetics and Modeling—Most transient kinetic experiments were performed at 25 °C in an Applied Photophysics stopped-flow spectrophotometer with a dead time of 1.2 ms. A monochromator with a 2-nm bandpass was used for fluorescence excitation, and a 395-nm cutoff filter was used to measure fluorescence emission. The mant-labeled nucleotides were excited by FRET from endogenous tryptophan residues (290 nm); pyrene actin was excited at 365 nm, and phosphate-binding protein was excited at 380 nm. Nonlinear least squares fitting of the data were conducted on software provided with the instrument or KaleidaGraph. The DdMII studies were performed in a Biokine (Biologic) stopped-flow apparatus, and tryptophan fluorescence was observed with an excitation wavelength of 297 nm, and emission was measured with a 340-nm interference filter. The DdMII stopped-flow experiment was performed at 13 °C to maximize the tryptophan fluorescence signal. Reported uncertainties correspond to standard errors of the fits unless noted otherwise. Kinetic results were interpreted in terms of Schemes 1 and 2 with a description of the methods used to fit each specific experiment given under "Results" and figure legends.

ATPase Assays—Steady state ATPase activities were assessed using an NADH enzyme-linked assay at 25 °C performed on the stopped flow (9, 34, 35). Absorbance changes were detected at 340 nm, and the extinction coefficient for NADH ($\epsilon_{340} = 6{,}220$ $M^{-1}\cdot cm^{-1}$) was used to determine the oxidation rate of NADH. Steady state ATPase rates were obtained at a set of $MgCl_2$ concentrations ranging from 0.5 to 10 mM (0.3 to 9 mM free Mg^{2+}, respectively) in the presence of 20 μM (MV) or 60 μM (SKII, SMII, NMIIA, and CMIIB) actin and saturating 1 mM ATP. Assays were also performed with a range of actin concentrations to determine maximum ATPase rate (k_{cat}) and the actin concentration at which ATPase is half-maximal (K_{ATPase}).

In Vitro Motility and Filament Breaking Assays—The actin filament sliding assay was performed as described previously (36) at a range of Mg^{2+} concentrations in conditions (controlled ionic strength) similar to the corresponding ATPase assay for each myosin. Myosin was adhered to a 1% nitrocellulose in an amyl acetate (Ladd Research)-coated coverslip directly or with a c-Myc antibody (Sigma) in the case of SMII and NMIIA. The surface was blocked with BSA at 1 $mg\cdot ml^{-1}$ before the addition of actin labeled with either rhodamine phalloidin (TRITC filter cube; excitation/emission, 545/620 nm) or Alexa (FITC filter cube; excitation/emission, 500/535 nm). An activation buffer with varying $MgCl_2$ concentrations (0.5–10 mM) was added containing MOPS or KMg50 with 5 μM calmodulin (MV only) and supplemented with the corresponding amount of KCl to maintain ionic strength and the following: 0.35% methylcellulose, 2.5 mM phosphoenolpyruvate, 20 units$\cdot ml^{-1}$ pyruvate kinase, 0.1 $mg\cdot ml^{-1}$ glucose oxidase, 5 $mg\cdot ml^{-1}$ glucose, 0.018 $mg\cdot ml^{-1}$ catalase, and 1 mM ATP. The slide was promptly viewed using a NIKON TE2000 microscope equipped with a 60×/1.4 NA phase objective and a Perfect Focus System. Images were acquired at intervals (0.2–5 s) and for periods of time (1–5 min) appropriate for each myosin using a shutter-controlled Coolsnap HQ2-cooled CCD digital camera (Photometrics) binned 2 × 2. Temperature was maintained at 26 ± 1 °C and monitored using a thermocouple meter (Stable Systems International). Image stacks were transferred to ImageJ for analysis via MTrackJ (37). Frequency of filament breakage was determined for MV, NMIIA, and SKII at 0.3 and 9.0 mM free Mg^{2+} by recording elapsed time to initial filament breakage for ≥50 filaments per condition (38).

Pig Myocardial Strips—All procedures were reviewed and approved by the Institutional Animal Care and Use Committees of the University of Vermont College of Medicine. Cardiac papillary muscle was taken from one male conventional swine (E. M. Parsons) weighing 16 kg. Myocardial strips were dissected further, chemically skinned, and studied at 27 °C as described previously (39). Free Mg^{2+} concentrations of 1, 2, 4, and 8 mM were applied at *p*Ca 4.8 by exchanging volumes of 1 or 8 mM free Mg^{2+} solutions.

Chemicals and reagents were obtained from Sigma, and concentrations were expressed in $mmol\cdot liter^{-1}$ unless noted otherwise. Concentrations were calculated using an ionic equilibrium program (40). Relaxing solution was as follows: *p*Ca 8.0, 20 *N,N*-bis(2-hydroxyethyl)-2-aminoethanesulfonic acid, 1 EGTA, 4 MgATP, 1 free Mg^{2+}, 35 phosphocreatine, 300 units ($\mu mol\ P_i\cdot min^{-1})\cdot ml^{-1}$ creatine kinase, 1 mM DTT, ionic strength 200 mEq adjusted with sodium methane sulfate, pH 7.0. Activation solution was the same as relaxing with 1 or 8 mM free Mg^{2+} and *p*Ca 4.8.

Sinusoidal length perturbations of amplitude 0.125% muscle strip length were applied over 0.125–250 Hz. The elastic and viscous moduli were measured from the tension response, and Equation 2 was fitted to the complex modulus,

$$\tilde{Y}(\omega) = A(i\omega)^k - B\left(\frac{i\omega}{2\pi b + i\omega}\right) + C\left(\frac{i\omega}{2\pi c + i\omega}\right) \quad \text{(Eq. 2)}$$

where *A*, *B*, and *C* are magnitudes expressed in $kilonewtons\cdot m^{-2}$; *k* is a unit-less exponent; *b* and *c* are characteristic frequencies expressed in Hz; ω is angular frequency in units of s^{-1} of the length perturbation equal to 2π × frequency of perturbation, and $i = (-1)^{1/2}$. The rate $2\pi c$ is the equivalent of the myosin cross-bridge detachment rate, and its reciprocal is equal to time on, and the average time myosin is attached to actin (39).

RESULTS

To investigate the impact of Mg^{2+} on actomyosin mechanochemistry, we examined the Mg^{2+} dependence of a subset of

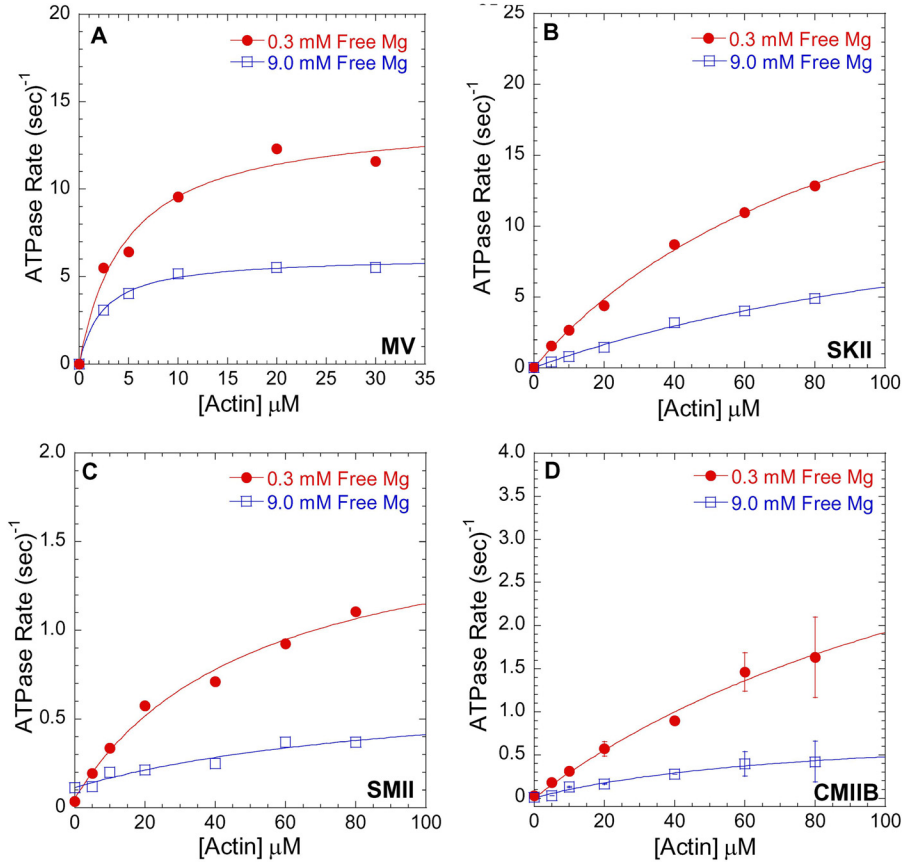

FIGURE 1. **Mg^{2+}-dependent actin-activated ATPase activity.** ATPase assays were performed in ionic strength controlled conditions with 0.3 mM free Mg^{2+} (*filled red circles*) or 9.0 mM free Mg^{2+} (*open blue squares*) for MV (*A*), SKII (*B*), SMII (*C*), and CMIIB (*D*) in the presence of different actin concentrations at 25 °C. See Table 1 for a summary of k_{cat} and K_{ATPase} values.

myosins in three assays as follows: actin-activated ATPase, *in vitro* motility, and transient kinetic determination of the ADP release rate constant (Figs. 1-4). We examined a processive high duty ratio motor (MV), two class II myosins with relatively slow ADP release rate constants (NMIIA and SMII), and two low duty ratio muscle myosins (CMIIB and SKII). All assays were performed in ionic strength-controlled conditions by varying the concentration of KCl to offset the difference in $MgCl_2$ concentration.

Actin-activated ATPase Activity—Ionic strength-controlled steady state actin-activated ATPase assays for MV (Fig. 1*A*), SKII (Fig. 1*B*), SMII (Fig. 1*C*), and CMIIB (Fig. 1*D*) were performed at 1 and 10 mM $MgCl_2$ (0.3 and 9.0 mM free Mg^{2+}, respectively) and a range of actin concentrations. The analysis allowed for determination of the maximum actin-activated ATPase activity (k_{cat}) and the actin concentration at which the ATPase activity is half-maximal (K_{ATPase}) at low (0.3 mM) and high (9.0 mM) free Mg^{2+} concentrations. SKII and SMII exhibited an approximate 2-fold decrease in k_{cat} accompanied by a 2-fold increase in K_{ATPase} at 9 mM free Mg^{2+} (Table 1). MV and CMIIB exhibited a 2- and 6-fold decrease in k_{cat}, respectively, and a 2-fold decrease in K_{ATPase} at 9 mM free Mg^{2+}. All class II myosins demonstrated a 3-fold reduction in k_{cat}/K_{ATPase} at high Mg^{2+}, although MV was unchanged.

ADP Release Rate Constant—The Mg^{2+} dependence of the ADP release rate constant was examined directly by monitoring the dissociation of mant-dADP in MV (Fig. 2*A*), NMIIA (Fig. 2*B*), and SMII (Fig. 2*C*). A complex of actomyosin·mant-dADP was mixed with saturating ATP (final conditions: 0.75–1 μM actin, 0.5–0.75 μM myosin, 10–20 μM mant-dADP, and 1 mM ATP). The mant-dADP fluorescence transients followed a single exponential in SMII and a double exponential in MV and NMIIA as reported previously (24, 26, 27). The fast phase of the ADP release rate constants in MV and NMIIA was more steeply dependent on Mg^{2+} concentration. The ADP release rate constants (fast phase for MV and NMIIA) were reduced ~2-fold at

TABLE 1

Summary of k_{cat} (maximum ATPase rate) and K_{ATPase} (actin concentration at half-maximal activation) values for actin-activated ATPase at 0.3 and 9 mM free Mg^{2+}, determined by fitting the data in Fig. 1 to Michaelis-Menten kinetics

	k_{cat} (s^{-1})		K_{ATPase} (μM)	
Myosin Isoform	0.3 mM	9 mM	0.3 mM	9 mM
MV	14±1.0	6.1±0.1	4.7±1.1	2.4±0.3
SKII	29.3±3.0	15.6±3.3	101.0±16.0	171.8±50.0
SMII	1.7±0.2	0.6±0.4	51.7±18.0	102.0±113.1
CMBII	5.0±1.5	0.8±0.2	161.4±64.8	77.0±26.3

	k_{cat}/K_{ATPase} ($\mu M^{-1}\cdot s^{-1}$)	
Myosin Isoform	0.3 mM	9 mM
MV	2.98±0.22	2.54±0.67
SKII	0.29±0.07	0.09±0.03
SMII	0.03±0.02	0.01±0.01
CMBII	0.03±0.01	0.01±0.01

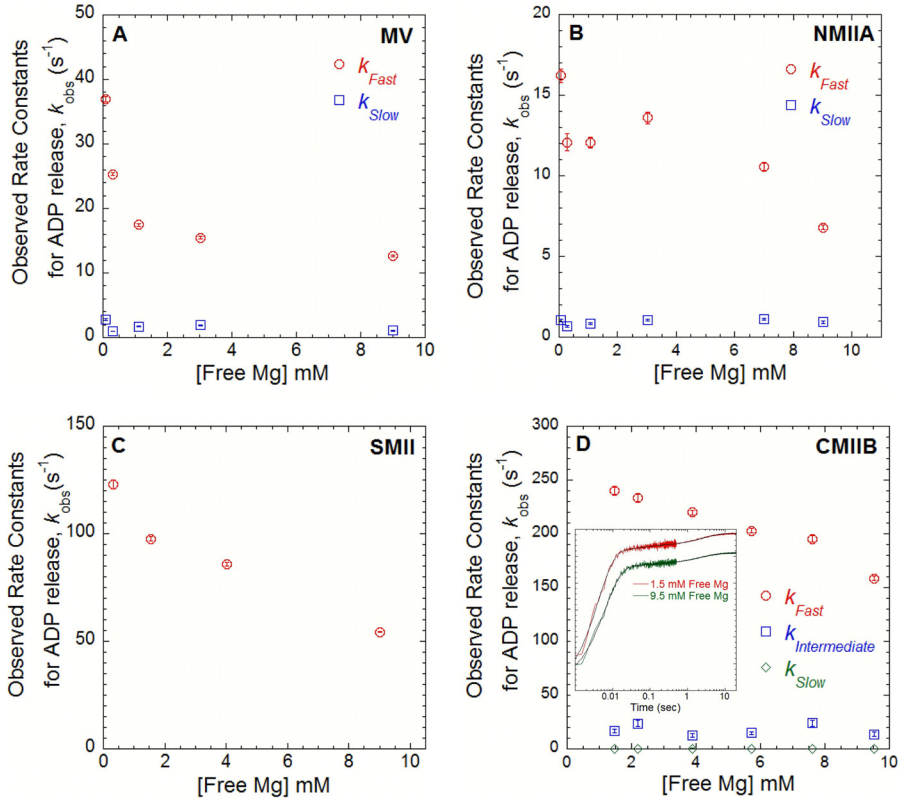

FIGURE 2. **Mg^{2+}-dependent ADP release in MV, NMIIA, SMII, and CMIB.** The ADP release rate constants were examined by mixing acto-MV (*A*), -NMIIA (*B*), and -SMII (*C*) in the presence of mant-dADP with 1 mM ATP. The free Mg^{2+} was varied between 0.3 and 9 mM at 25 °C (final reaction conditions: 0.5–0.75 μM myosin, 0.75–1 μM actin, 10–20 μM mant-dADP, and 1 mM ATP). *D*, ADP release rate constant was measured in CMBII by performing ATP-induced dissociation from pyrene actin in the presence of ADP. A complex of pyrene acto-CMIIB·ADP was mixed with ATP, and the resulting fluorescence transients (see *inset*) were best fit by a three-exponential function (final reaction conditions: 0.8 μM CMIIB and pyrene actin, 160 μM ADP, and 16 mM ATP). The observed rates of the fast, intermediate, and slow phases are plotted as a function of free Mg^{2+} concentration. The relative amplitudes were similar at all free Mg^{2+} concentrations measured (fast = 0.9, intermediate = 0.02, and slow = 0.08).

9.0 mM as compared with 0.3 mM free Mg^{2+} and are shown for MV (Fig. 2*A*, *open red circles*), NMIIA (Fig. 2*B*, *open red circles*), and SMII (Fig. 2*C*). The relative amplitudes of the double exponential fits with MV (83% fast phase) and NMMIIA (74% fast phase) were similar at all free Mg^{2+} concentrations examined. To measure the ADP release rate constant in CMIIB, we examined ATP-induced dissociation from pyrene actin in the presence of ADP (Fig. 2*D*). Pyrene actin is quenched when myosin is strongly bound, and ATP binding allows examination of the rate of transition into the weakly bound states. A complex of pyrene actin·CMIIB in the presence of ADP was mixed with high concentrations of ATP, and the free Mg^{2+} concentrations were varied (final conditions: 0.8 μM pyrene actin and CMIIB, 160 μM ADP, and 16 mM ATP). The transients were best fit by a three exponential function, and only the fast phase was dependent on free Mg^{2+}. The relative amplitudes of the three phases were not Mg^{2+}-dependent. Therefore, the fast phase was modeled to be the ADP release rate constant; the intermediate phase was modeled to be the previously identified slow isomerization in the nucleotide binding pocket (41), and the slow phase was a nonspecific fluorescence change. The ADP release rate constants were about 2-fold faster than previous measurements performed at 20 °C and slightly different buffer conditions (41, 42).

Because the ADP release rate constant is extremely fast in SKII, we measured the ADP affinity in CMIIB and SKII (Fig. 3, *A* and *B* and *C* and *D*, respectively). The ADP affinity at four different free Mg^{2+} concentrations was measured by competition with ATP-induced dissociation monitored by pyrene actin fluorescence (43). At each free Mg^{2+} concentration, the rate of ATP-induced dissociation was measured in the absence and presence of different concentrations of ADP. The transients (k_{obs}) were fit to a single exponential function, and the rate of ATP-induced dissociation decreased as a function of ADP concentration present. The rate constants were normalized to the rate in the absence of ADP (k_{rel}) (where $k_{rel} = k_{obs}/k_0$ and $k_0 = k_{obs}$ in the absence of ADP) and plotted as a function of ADP concentration. The k_{rel} was plotted as a function of ADP concentration for CMIIB (Fig. 3, *A* and *B*) and SKII (Fig. 3, *C* and *D*). The data were fit to a previously established equation ($k_{rel} = 1/(1 + [ADP]/K'_{ADP})$), where K'_{ADP} is the apparent affinity for ADP (42), which was slightly enhanced at higher free Mg^{2+} concentrations in SKII ($K'_{ADP} = 271 \pm 26$, 291 ± 22, 247 ± 22, and 201 ± 23 at 0.3, 1.1, 3, and 9 mM free Mg^{2+}, respectively) and relatively insensitive to Mg^{2+} in CMIIB ($K'_{ADP} = 83 \pm 16$, 80 ± 15, 73 ± 15, and 91 ± 23 at 0.3, 1.1, 3, and 9 mM free Mg^{2+}, respectively).

Actin-activated ATPase Activity and in Vitro Motility—The actin-activated ATPase assay was performed in the presence of 20 μM (MV) or 60 μM (class II myosins) actin and 1 mM ATP at a range of free Mg^{2+} concentrations (Fig. 4). The ADP release rate constant is the rate-limiting step in the MV solution

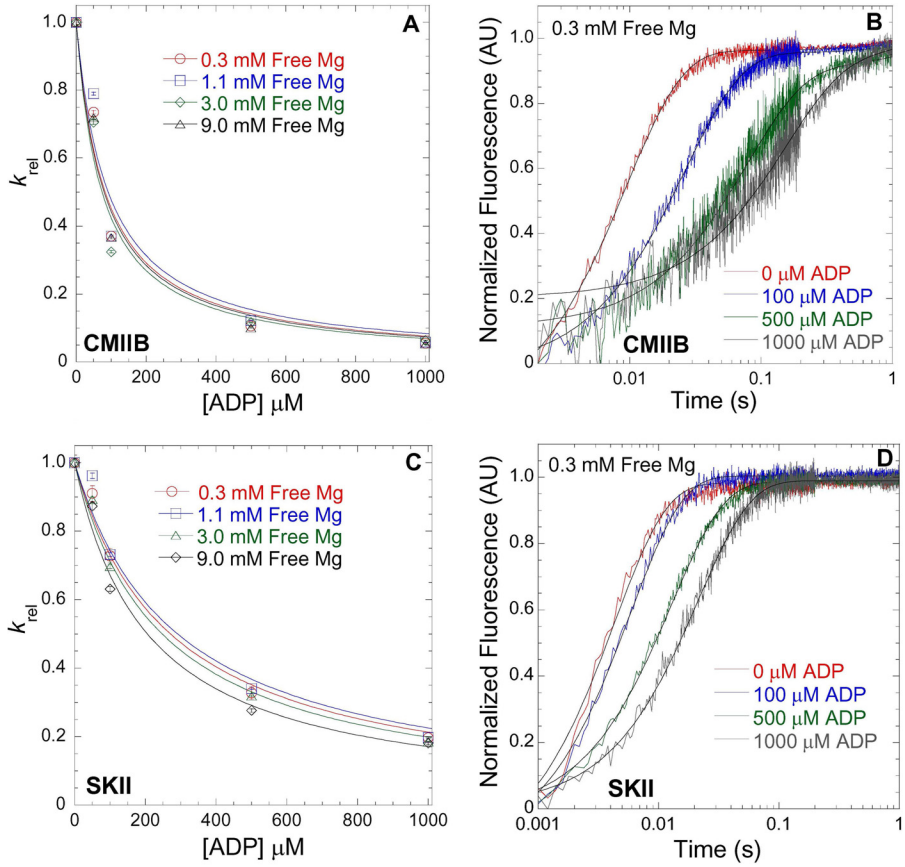

FIGURE 3. **Mg^{2+}-dependent ADP affinity in CMIIB and SKII.** ATP-induced dissociation from pyrene actin in the presence of ADP was utilized to measure the ADP affinity in CMIIB (*A*) and SKII (*C*) in the presence of 0.3, 1.1, 3.0, and 9.0 mM free Mg. The fluorescence (arbitrary units, *AU*) transients were fit to a single exponential, and the k_{rel} ($k_{rel} = k_{obs}/k_0$, where $k_0 = k_{obs}$ in the absence of ADP) values were plotted as a function of [ADP]. The ADP affinity was determined from the hyperbolic fits ($k_{rel} = 1/(1 + [ADP]/K'_{ADP}$, where K'_{ADP} = the apparent affinity for ADP) at each free concentration as is shown for 0.3 mM free Mg in CMIIB (*B*) and SKII (*D*) (final reaction conditions: 0.5 μM myosin, 1 μM pyrene actin, 50 μM ATP, and varying concentrations of ADP).

ATPase assay, whereas attachment to actin or phosphate release are rate-limiting in the ATPase assay for class II myosins (23). We can therefore begin to elucidate which step(s) in the myosin ATPase cycle are impacted by Mg^{2+} based on trends in the ATPase and *in vitro* motility assays, as well as the relative changes in the ADP release rate constant. The ATPase assays for myosin V and all four class II myosins were dependent on Mg^{2+}; however, MV was more steeply dependent on Mg^{2+}. The *in vitro* motility sliding velocities exhibited similar magnesium dependences to the corresponding ATPase assay for all five myosins examined. The Mg^{2+} dependence of the ADP release rate constant for MV, NMIIA, SMII, and CMIIB followed a similar trend as the *in vitro* motility assays. The ADP affinity of SKII (Fig. 4*B*), which was fairly insensitive to free Mg^{2+}, was also plotted for comparison.

Kinetic Mechanism of Mg^{2+}-dependent ADP Release in DdMII Motor—To further examine how Mg^{2+} alters the kinetics of the myosin·ADP states, we performed transient kinetic studies with single tryptophan containing DdMII motor constructs. We examined the fluorescence changes in Trp-239 located in the switch I region, which decreases in fluorescence (15%) upon ADP binding. We also examined Trp-501 in the relay helix, which also decreases (15%) in fluorescence upon ADP binding. The rates of binding and release were monitored with both constructs. Similar values for the second-order rate constant (k_{+ADP}) and the dissociation rate constant (k_{-ADP}) were obtained with both constructs. The second-order rate constant for ADP binding to myosin was increased 10–20-fold in the absence of Mg^{2+}, although the dissociation rate constant was also increased 10-fold in the presence of saturating Mg^{2+} (20 mM $MgCl_2$) (Table 2 and Figs. 5 and 6). Our previous results (3) and the results in Fig. 7*C* are consistent with 20 mM $MgCl_2$ being saturating in DdMII. The rate of Mg^{2+} binding to myosin·ADP was monitored with Trp-239 fluorescence (Fig. 7). We observed a fluorescence increase followed by a decrease upon Mg^{2+} binding, and the rates and amplitudes were dependent on Mg^{2+} concentration. Analysis of the data allowed for the determination of the rates of association, dissociation, and overall affinity. A summary of DdMII ADP states in the presence and absence of Mg^{2+} satisfies the thermodynamic law of detailed balance (Scheme 2). Therefore, the overall affinity for ADP is relatively insensitive to Mg^{2+} in DdMII, similar to what was observed in SKII and CMBII. The 10-fold faster rate constant for ADP dissociation in the absence of Mg^{2+} is similar to what was observed in myosin V, although the impact on the second-order rate constant for ADP binding was less pronounced in myosin V (3-fold) (9). The basal ATPase activity is not altered by Mg^{2+} in DdMII (0.03 s^{-1} at both 0.17 mM and 20 mM $MgCl_2$), which is consistent with Mg^{2+} only altering the ADP release step in the absence of actin, which is not rate-limiting (44).

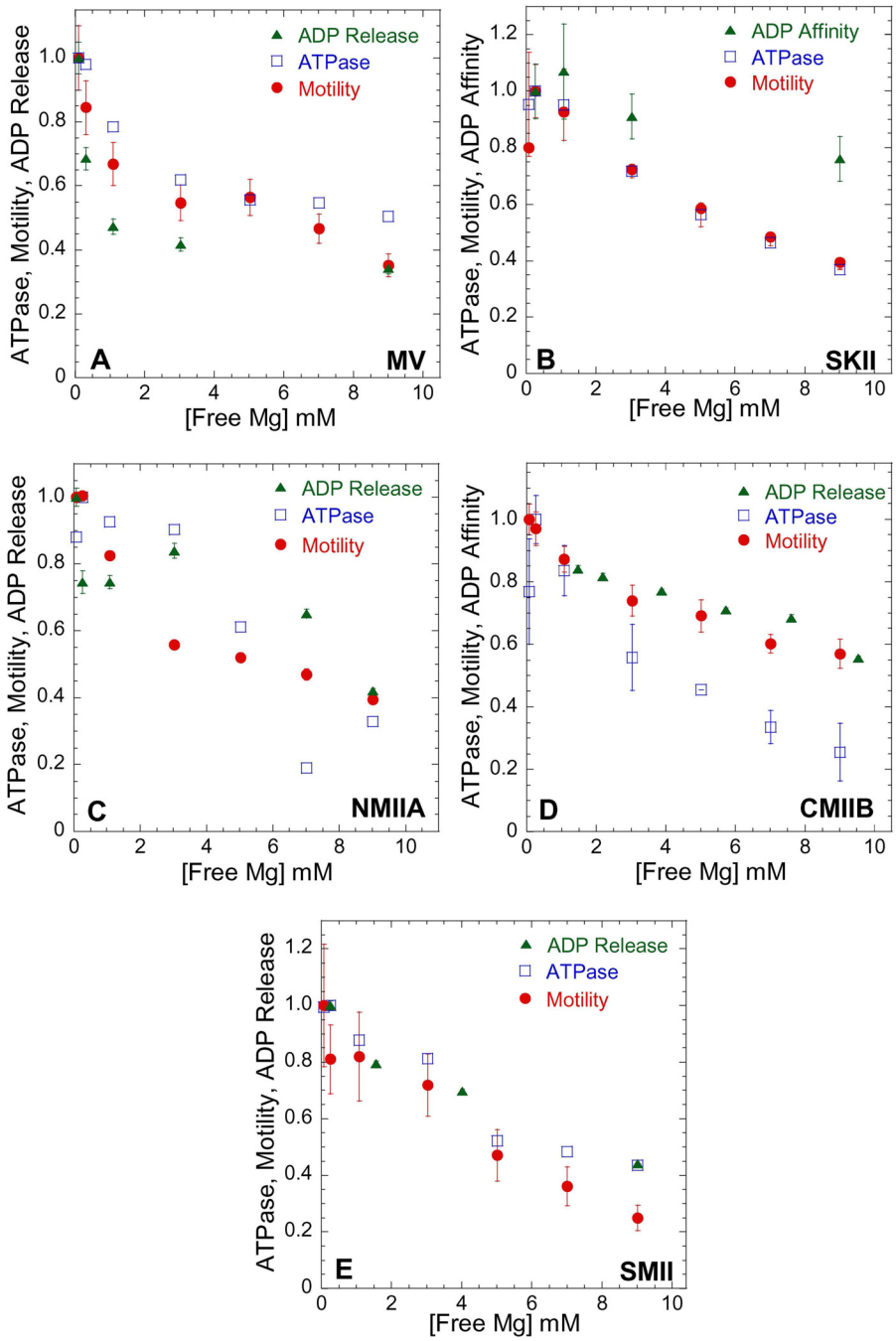

FIGURE 4. **Influence of Mg^{2+} on actomyosin ATPase, motility, and ADP release/affinity.** Steady state ATPase (*open blue squares*), motility (*filled red circles*), and ADP release/affinity (*filled green triangles*) were performed in ionic strength-controlled conditions with 0.3–9.0 mM free Mg for MV (*A*) and members of the myosin II family as follows: SKII (*B*); NMIIA (*C*); CMIIB (*D*); and SMII (*E*). The ATPase assays were performed at 25 °C with fixed actin concentrations in MV (20 μM actin) and MII (60 μM actin). Actomyosin motility was performed at 27 °C (see Table 4 for velocity values). The data are expressed as relative values for comparison (normalized to the value obtained at 0.3 mM free Mg). The ADP release rate constant was examined with mant-dADP or pyrene actin (see Fig. 2), and ADP affinity was measured by competition with ATP-induced dissociation (see Fig. 3).

Actin-activated Phosphate Release—To attempt to identify other steps in the actomyosin ATPase cycle altered by Mg^{2+}, the phosphate release rate constant was examined at 0.3 and 9 mM free Mg^{2+} in single-headed myosin V (MV 1IQ) at a range of actin concentrations (2.5–30 μM). MV 1IQ was mixed with ATP, aged for 5 s, and then mixed with actin (final concentrations: 0.25 μM MV, 0.2 μM ATP, 4 μM phosphate-binding protein, and varying actin concentrations). The fluorescence transients were fit to a single exponential function. The plots of phosphate release rate constant as a function of actin concentration were fit to a hyperbolic function to determine the affinity for actin in the M·ADP·P_i state ($1/K_9$) and maximum rate of phosphate release (k'_{+4}) (Fig. 8). The kinetics of actin-activated phosphate release at 0.3 mM free Mg^{2+} are similar to previous reports ($1/K_9 = 3.2$ μM, $k'_{+4} = 106$ s^{-1}) (10, 45). In the presence of 9 mM free Mg^{2+}, the actin affinity in the M·ADP·P_i state was 5-fold weaker ($1/K_9 = 16.8$ μM), although the rate of phosphate release was unchanged ($k'_{+4} = 125$ s^{-1}).

TABLE 2

Summary of rate and equilibrium constants for ADP binding measured with the single tryptophan containing DdMII constructs in the absence of $MgCl_2$ or in the presence of 20 mM $MgCl_2$

	*0 mM $MgCl_2$	20 mM $MgCl_2$
Rate or Equilibrium Constant		
	W501	*W501*
$k_{-ADP}(s^{-1})$	[a]47 ± 29	[b]2.8 ± 0.6
$k_{+ADP}(\mu M \cdot s^{-1})$	[a]3.5 ± 0.1	[b]0.35 ± 0.01
K_{ADP} (μM) (k_{-ADP}/k_{+ADP})	13	8.1
K_{ADP} (μM)	[c]14 ± 3	[c]8.7 ± 1.9
	W239	*W239*
$k_{-ADP}(s^{-1})$	[a]40 ± 50	[b]6.0 ± 1.4
$k_{+ADP}(\mu M \cdot s^{-1})$	[a]5.5 ± 1.5	[b]0.34 ± 0.21
K_{ADP} (μM) (k_{-ADP}/k_{+ADP})	7.2	18
K_{ADP} (μM)	[c]23 ± 5	[c]6 ± 2

* 0.5 mM EDTA was used to chelate any residual Mg.
[a] Data were determined from hyperbolic fit to data in Fig. 5, *C* and *D*.
[b] Data were determined from hyperbolic fit to data in Fig. 6, *C* and *D*.
[c] Data determined from hyperbolic fit to data in Figs. 5, *E* and *F* or 6, *E* and *F*.

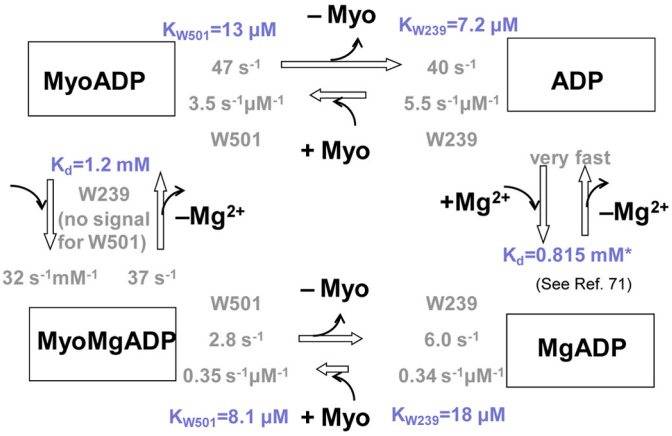

Scheme 2.

Filament Breaking Assay—An *in vitro* motility filament-breaking assay was performed by measuring the average time to initial filament breakage in MV, NMIIA, and SKII (Table 3). Filament breaking analysis showed a 2-fold reduction in time to initial breakage at 9 mM free Mg^{2+} compared with 0.3 mM free Mg^{2+} in all three myosins. Although we cannot rule out that the increased free Mg^{2+} alters the stability of the actin filaments, we found the actin filament lengths were similar at low and high free Mg^{2+} (8 ± 1 μm) examined in the absence of ATP. The filament breaking results indicate that the attached time is increased at high free Mg^{2+} concentrations, and the results parallel the relative reduction in ADP release rate constant observed for MV and NMIIA.

Pig Myocardial Mechanics and Kinetics—Fig. 9, *A* and *B*, illustrates the influence of varying free Mg^{2+} concentrations on the elastic and viscous moduli, respectively. As the free Mg^{2+} concentration was elevated from 2 to 8 mM, the elastic and viscous moduli shifted to lower frequencies. When the Mg^{2+} concentration was then lowered to repeat the 2 mM condition, the moduli shifted back to higher frequencies, thus verifying reversibility of the effects.

The myosin cross-bridge detachment rate $2\pi c$ was significantly lowered with increasing Mg^{2+} concentrations (Fig. 9*C*). These data reflect a longer myosin cross-bridge attached time as a function of increased free Mg^{2+} concentration (Fig. 9*D*). Because ATP concentrations are saturating, the detachment rate measured here reflects the ADP release rate constant of the myosin cross-bridge. We did not detect any significant effect of Mg^{2+} on developed tension (Fig. 9*E*). Our results here are qualitatively similar to those for skinned rat cardiac muscle reported by Puchert *et al.* (46), who report slower characteristics of force redevelopment as free Mg^{2+} is raised from 0.5 to 1 mM. Our observations of the effects of free Mg^{2+} concentration on cross-bridge ADP release rate constant in the skinned myocardial strip demonstrate that the findings in isolated pig cardiac myosin are detectable within the context of an intact myofilament lattice.

DISCUSSION

By examining the Mg^{2+} dependence of a number of muscle and nonmuscle myosins, we demonstrate that conserved mechanisms likely mediate the impact of free Mg^{2+} on the myosin mechanochemical cycle. It is well established that the ADP release rate constant plays a critical role in influencing the period of time myosin remains attached to actin in the presence of physiological ATP concentrations and therefore correlates with unloaded shortening velocity. Our current results demonstrate that the slowing of the ADP release rate constant as a function of increasing free Mg^{2+} concentration is a conserved feature of myosin motors. We also find that Mg^{2+} can alter the attachment of myosin to actin in the post-hydrolysis M·ADP·P_i state, measured directly in myosin V. Our overall observations and analysis at the molecular level are consistent with our findings in skinned muscle fibers that demonstrate free Mg^{2+} reduces the ADP release rate constant within the context of an intact myofilament lattice and would be expected to reduce contractile velocity of activated muscle while not altering overall muscle tension.

Impact on Detachment-limited Actomyosin Motility—We found that in the myosins examined, the Mg^{2+} dependence of the *in vitro* motility sliding velocity and the ADP release rate constant followed a similar trend (Fig. 4). The relationship between ADP release and actomyosin motility has been well established (41, 43, 47). Our previous results demonstrated that the temperature dependence of *in vitro* motility also followed a similar trend to the temperature dependence of the ADP release rate constant (24). Overall, Mg^{2+} dependence of *in vitro* sliding velocity can mostly be explained by a detachment-limited mechanism of motility. The detachment rate ($1/t_{on}$) at low and high Mg^{2+} can be calculated using the *in vitro* sliding velocities (V) and the literature values of the working stroke (d_{uni}) (MV (48); SKII (49), SMII (50), NMII (51), and CMIIB (52)). In MV, NMIIA, CMIIB, and SMII, the calculated detachment rates are within 2–3-fold of the measured ADP release rate constants (Table 4). Differences between the calculated and measured detachment rates have been noted previously (51) and could result from a number of factors, including strain dependence of detachment or uncertainty in the working stroke values.

The release of ADP from actomyosin has been shown to be a two-step process in many myosins (10, 26). The first step is the isomerization of the nucleotide binding pocket from a closed to an open conformation followed by local structural changes in the

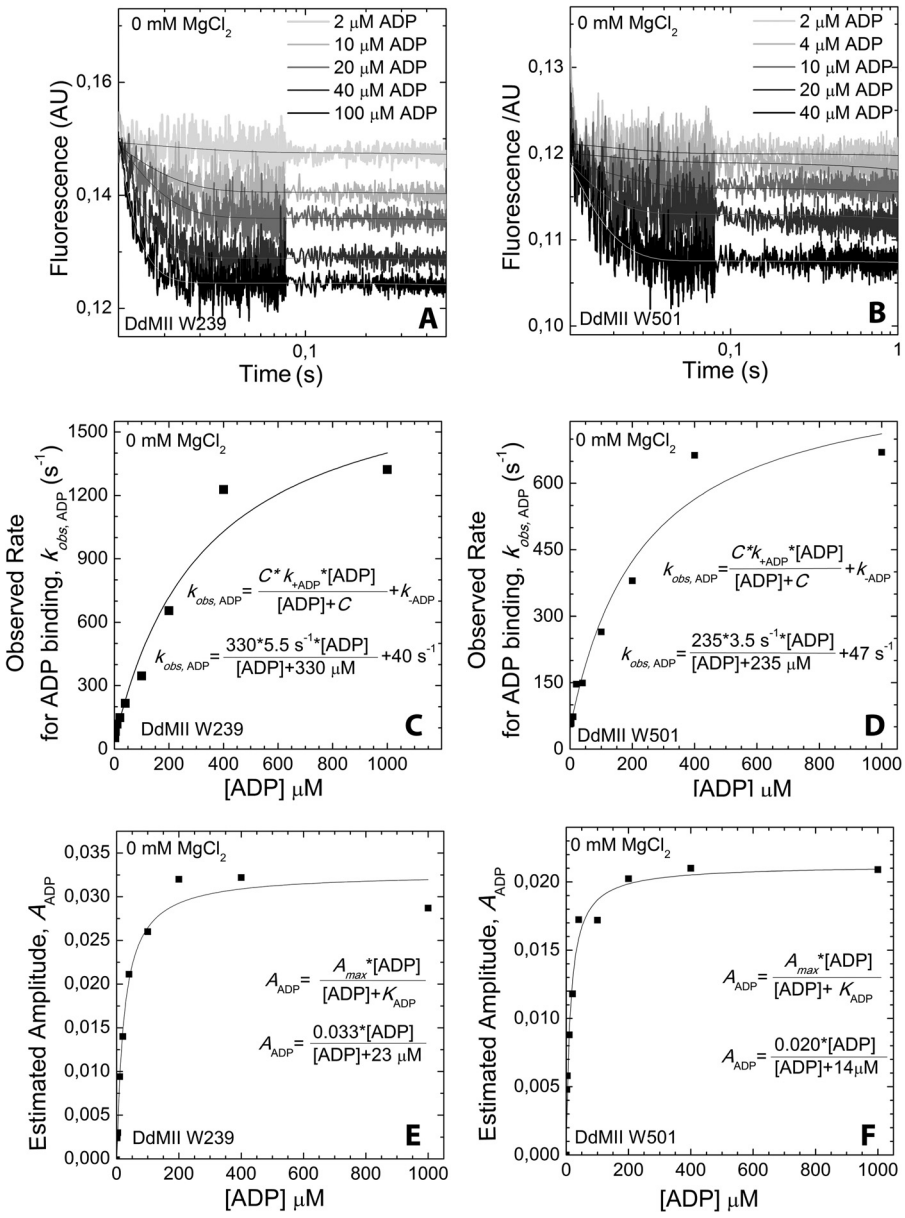

FIGURE 5. **ADP binding to DdMII motor domain in the absence of Mg^{2+}.** Trp-239 DdMII (*A*) and Trp-501 DdMII (*B*) fluorescence (arbitrary units, *AU*) transients upon binding with increasing concentrations of ADP are shown. Mixing conditions are as follows: 3–5 μM DdMII was mixed with increasing concentrations of ADP; both syringes contained 20 mM HEPES, 120 mM NaCl, and 0.5 mM EDTA, pH 7.3, buffer at 13 °C. Single exponential decays were fitted to the averages of 3–5 measurements. ADP concentration dependence of the fitted observed rates is shown for Trp-239 DdMII (*C*) and Trp-501 DdMII (*D*). The ADP binding to DdMII motor domain was treated kinetically as a second-order reaction. The observed rate constants fit a hyperbolic function of ADP concentration. The hyperbolic fit is indicated on each *graph; C* is the negative vertical asymptote; k_{+ADP} and k_{-ADP} are the binding and unbinding rate constants, respectively. ADP concentration dependence of the amplitudes of the fluorescent transients is also shown for Trp-239 DdMII (*E*) and Trp-501 DdMII (*F*). Amplitudes were estimated from the offsets of the transients, because the dead time of the stopped-flow apparatus (~0.3 ms) results in a considerable amplitude loss in the fits. K_{ADP}, the ADP affinity of DdMII, is calculated from the hyperbolic ADP concentration dependence of the amplitudes. The calculated rate constants and ADP affinities from *C*, *D*, *E*, and *F* are summarized in Table 2.

active site required for the release of ADP. We and others have found that both steps are Mg^{2+}-dependent in myosin V (5, 6, 9) and that the isomerization step is rate-limiting in single-headed myosin V (9, 34). The second step is also quite steeply dependent on Mg^{2+} and may be the rate-limiting step in the myosin V dimer (53, 54). We observed a single exponential transient in the mant-dADP release studies with SMII, whereas the fluorescence transients with MV and NMIIA were best fit by a two-exponential function. We associated the fast phase of the ADP release transient with the nucleotide release step and found that this rate correlates well with the Mg^{2+} dependence of sliding velocity.

The ADP release kinetics in myosin V were more steeply dependent on free Mg^{2+} than the class II myosins examined (NMIIA, SMII, and CMIIB). Structural differences in the coordination of Mg^{2+} in the nucleotide binding pocket of class II and class V myosins may account for the differences observed in the Mg^{2+} concentration-dependent inhibition of ADP release. The class II myosins examined all have a serine instead of a tyrosine in the switch II region that was demonstrated to be important

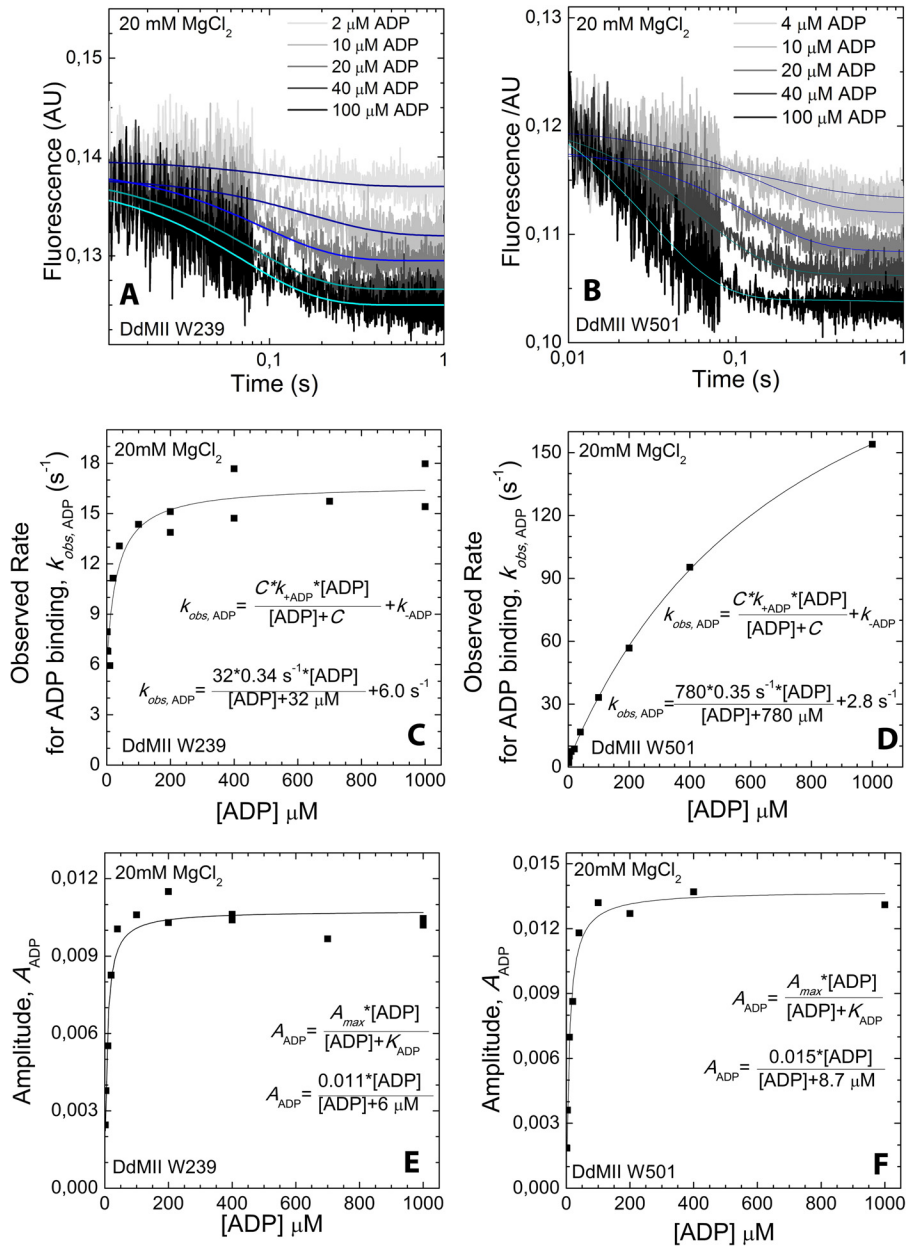

FIGURE 6. **ADP binding to DdMII motor domain in the presence of 20 mM $MgCl_2$.** Trp-239 DdMII (*A*) and Trp-501 DdMII (*B*) fluorescence (arbitrary units, *AU*) transients upon binding with increasing concentrations of ADP are shown. Mixing conditions are as follows: 3–5 μM DdMII was mixed with increasing concentrations of ADP; both syringes contained 20 mM HEPES, 60 mM NaCl, and 20 mM $MgCl_2$, pH 7.3 buffer, at 13 °C. Single exponential decays were fitted to the averages of 3–5 measurements. ADP concentration dependence of the fitted observed rates is shown for Trp-239 DdMII (*C*) and Trp-501 DdMII (*D*). The ADP binding to the DdMII motor domain was treated kinetically as a second-order reaction. The observed rate constants fit a hyperbolic function of ADP concentration. The hyperbolic fit is indicated on each *graph*; *C* is the negative vertical asymptote, and k_{+ADP} and k_{-ADP} are the binding and unbinding rate constants; respectively. ADP concentration dependence of the fitted amplitudes of the fluorescent transients is also shown for Trp-239 DdMII (*E*) and Trp-501 DdMII (*F*). K_{ADP}, the ADP affinity of DdMII is calculated from the hyperbolic ADP concentration dependence of the amplitudes. The calculated rate constants and ADP affinities from *C*, *D*, *E*, and *F* are summarized in Table 2.

for Mg^{2+} sensitivity (22). Our previous work demonstrated that the switch II region can play a role in mediating the transition between actomyosin·ADP states and the nucleotide release steps (55). The single tryptophan fluorescence experiments with DdMII demonstrate both switch I (Trp-239) and switch II (Trp-501) are sensitive to ADP binding (Figs. 5 and 6). The fluorescence of Trp-239 was sensitive to Mg^{2+} binding in the myosin·ADP state (Fig. 7). Also, the relative amplitudes of the fluorescence changes observed in both Trp-239 and Trp-501 upon ADP binding were greater in the absence of Mg^{2+}. Thus, our work highlights that both the switch I and switch II regions are critical for Mg^{2+} coordination in the myosin·ADP states, and further mutational analysis may determine other key residues responsible for mediating differences in Mg^{2+} affinity.

The ADP affinity measured in the striated muscle myosins (SKII and CMIIB) was relatively Mg^{2+}-insensitive. One possible explanation for these results is that both the ADP binding and ADP dissociation rate constants are Mg^{2+}-dependent, and thus the overall affinity is unchanged. The transient kinetic results with the single tryptophan containing DdMII constructs

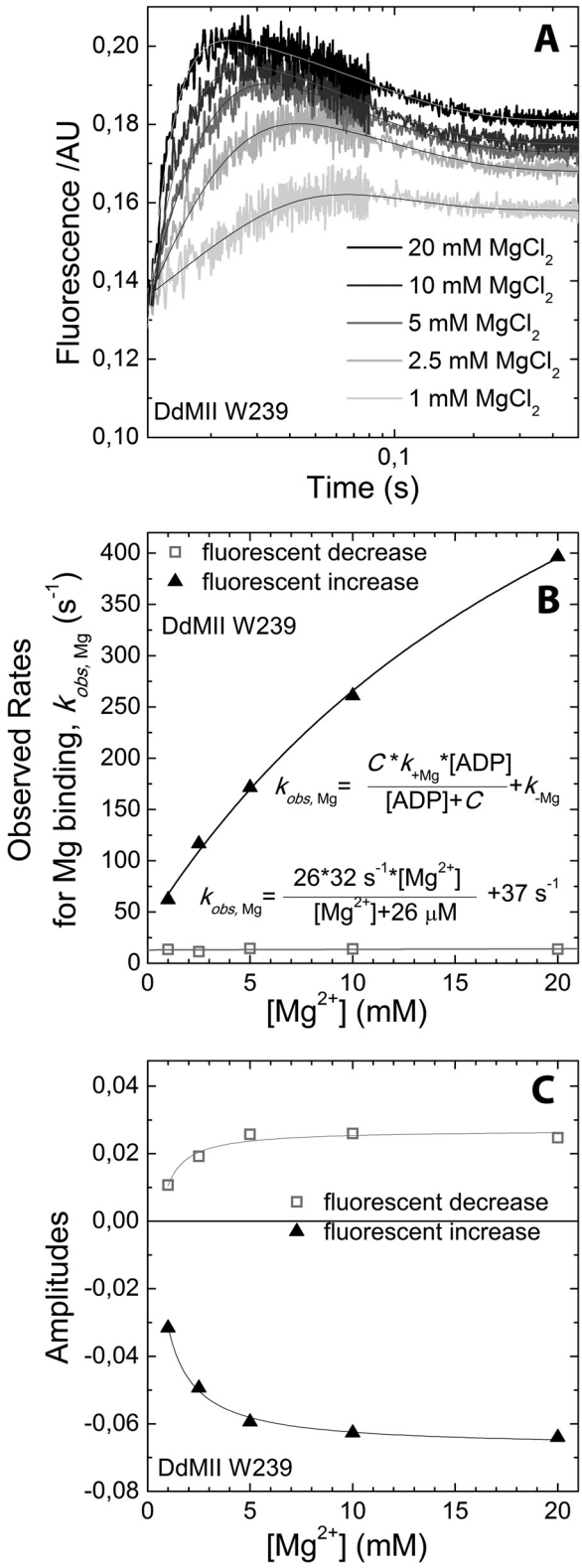

FIGURE 7. **Mg^{2+} binding to Trp-239 DdMII motor domain·ADP complex.** *A*, fluorescence (arbitrary units, *AU*) transients upon mixing ADP-bound DdMII with increasing concentrations of Mg^{2+}. Mixing conditions were as follows: 4 μM DdMII Trp-239, 1 mM ADP, 120 mM NaCl, 0.5 mM EDTA or 0–40 mM $MgCl_2$, and 0–120 mM NaCl; both syringes contained 20 mM HEPES, pH 7.3, at 13 °C. Double exponential decays were fitted to the averages of 3–5 measurements. *B*, Mg^{2+} concentration dependence of the fitted observed rate constants is shown. The rate of fluorescent decrease step is independent of Mg^{2+} concentration. The rate constants for Mg^{2+} binding and unbinding, k_{+Mg} and k_{-Mg}, are calculated from the Mg^{2+} dependence of the observed rate constant of the fluorescent increase and are summarized in Scheme 2 (the Mg affinity for free ADP was determined by Cahours *et al.* (71)). *C*, Mg concentration dependence of the fitted amplitudes of the fluorescent transients.

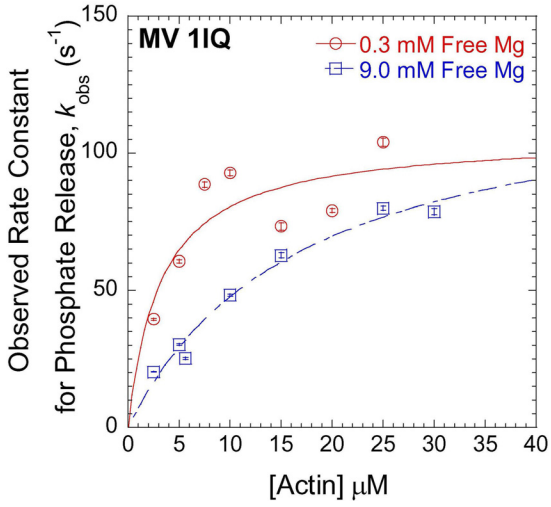

FIGURE 8. **Mg^{2+}-dependent phosphate release in MV 1IQ.** The phosphate release rate constants at 0.3 mM free Mg^{2+} (*open red circles*) and 9.0 mM free Mg^{2+} (*open blue squares*) were monitored by change in fluorescence of the phosphate-binding protein. MV 1IQ and sub-stoichiometric ATP were mixed and allowed to age for 10 s followed by the addition of actin in the presence of phosphate-binding protein (final reaction conditions: 0.25 μM MV 1IQ, 0.2 μM ATP, 4 μM phosphate-binding protein, and varying actin concentrations).

TABLE 3
Average time (seconds) to filament breakage at 0.3 and 9 mM free Mg

Myosin isoform	0.3 mM	9 mM
MV	106.5 ± 6.6	65.5 ± 5.7
NMIIA	95.4 ± 12.8	53.4 ± 4.5
SKII	20.8 ± 2.8	9.9 ± 1.6

demonstrate that this is indeed the case for DdMII. The second-order binding constant for ADP binding and the ADP release rate constant increase about 10–20-fold in the absence of Mg^{2+}, which results in relatively small changes in ADP affinity. However, the DdMII experiments were performed in the absence of actin, and the actin-bound conformations may alter Mg^{2+} sensitivity. A similar trend was observed in myosin V in the presence of actin, although the second order binding constant was more modestly increased 2–3-fold in the absence of Mg^{2+} (5, 6, 9).

Impact on Attachment to Actin—Our results demonstrate that the Mg^{2+} dependence of *in vitro* sliding velocity follows a similar trend as relative actin-activated ATPase rates. These results were surprising because the two assays are thought to have different rate-limiting steps for all of the class II myosins examined. Our results with MV 1IQ demonstrate that the phosphate release rate constant is not altered by Mg^{2+}, although the affinity for actin in the MV·ADP·P_i state is 5-fold weaker. The results suggest a mechanism for why the class II myosins examined had a reduced k_{cat}/K_{ATPase} at higher Mg^{2+}, because the rate-limiting step in these myosins is actin-activated phosphate release. We propose that Mg^{2+} could alter attachment to actin by changing the electrostatic interactions known to be important for formation of the initial interaction between actin and myosin (56, 57). Although the ionic strength

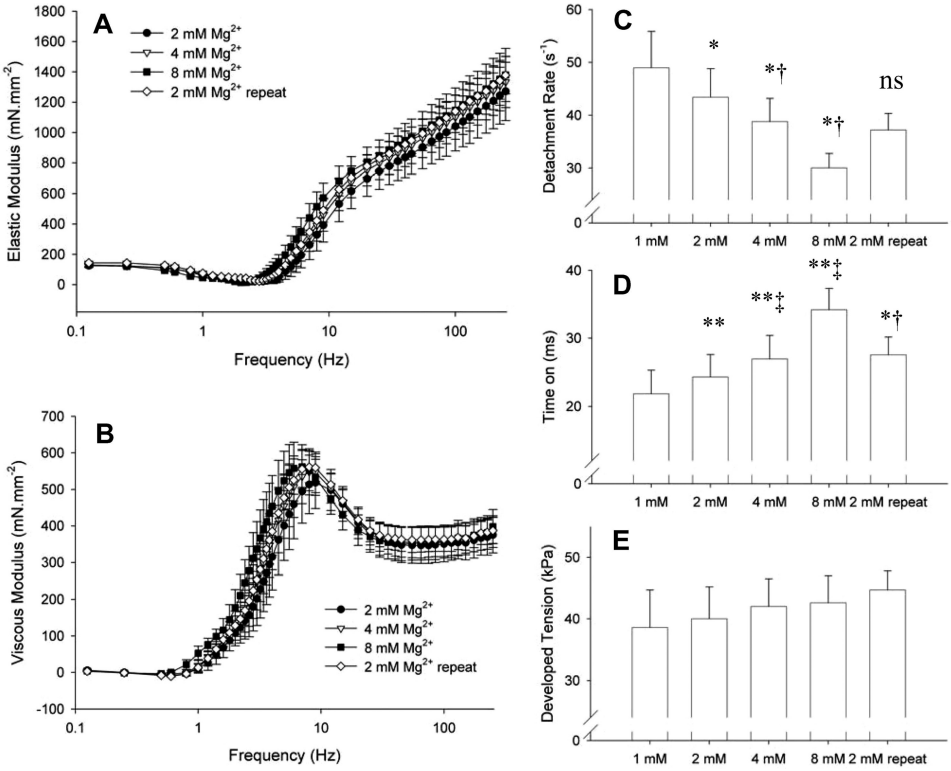

FIGURE 9. **Elastic and viscous moduli measured at maximum calcium activation and varying free Mg^{2+} concentrations.** *A* and *B*, characteristic dips and peaks of the elastic and viscous moduli were shifted to lower frequencies as free Mg^{2+} concentration was elevated. The repeat measurement at 2 mM free Mg^{2+} indicates that these effects were reversible. *C,* myosin cross-bridge detachment rate was detected by analysis of the frequency characteristics of the elastic and viscous moduli and was found to be reduced with increasing free Mg^{2+} concentrations. *D,* corresponding cross-bridge time-on was prolonged with increasing free Mg^{2+} concentrations. *E,* developed isometric tension was not significantly affected by Mg^{2+}. One-way analysis of variance demonstrated significance at $p < 0.01$ level for detachment rate and time on. *rep* = repeat. *, $p < 0.05$; **, $p < 0.01$ compared with 1 mM condition, and †,$p < 0.01$ compared with 8 mM condition by paired *t* test. $n = 4$ strips.

TABLE 4

Comparison of velocity and detachment rates at low and high free Mg

	Velocity (nm/s)[a]		$1/t_{on}$ (s^{-1})[b]		ADP release (s^{-1})[c]	
Myosin isoform	Low	High	Low	High	Low	High
MV	368 ± 9	153 ± 8	14.8 ± 0.4	6.1 ± 0.3	25.3 ± 1.0	12.7 ± 1.1
SKII	5050 ± 127	1984 ± 74	1010 ± 25.3	396.9 ± 14.9	ND	ND
NMIIA	231 ± 2	91 ± 3	46.2 ± 0.5	18.2 ± 0.6	12.1 ± 0.3	6.8 ± 0.1
CMIIB	645 ± 89	420 ± 103	108 ± 15	70 ± 17	226 ± 2.9	149 ± 1.7
SMII	503 ± 14	154 ± 5	100.6 ± 2.8	30.9 ± 1.1	123 ± 2.0	54.3 ± 0.3

[a] Sliding velocities were determined in the *in vitro* motility assay in the presence of low free Mg (0.3 mM for all except CMIIB, which is shown at 1.1 mM free Mg for comparison with ADP release) and high free Mg (9 mM).
[b] Data were determined by $(1/t_{on}) = V/d_{uni}$, where d_{uni} was taken from the literature values referenced in the text.
[c] Data were determined from the mant-dADP release studies in MV (fast phase), NMIIA (fast phase), SMII (free Mg is the same as velocity and $1/t_{on}$), and pyrene-actin experiments in CMIIB (low free Mg = 1.5 mM and high free Mg = 9.5 mM).

was held constant in our studies, there may be differences in how divalent and monovalent cations impact charged interactions in the actomyosin interface. Alternatively, Mg^{2+} could alter a conformational change in the actin binding region prior to phosphate release, such as closure of the actin-binding cleft. Our previous work demonstrated a rapid structural change in the actin binding region prior to phosphate release in myosin V (58), and this conformational change could be slowed by Mg^{2+} binding to an allosteric site.

The work of Baker and co-workers (38, 59) suggests that myosins can follow attachment-limited motility under certain conditions (*e.g.* high ionic strength and low motor density). We considered the possibility that the impact of Mg^{2+} on the attachment rate can play a role in altering sliding velocity in class II myosins. Baker and co-workers (38) have proposed a mechanism to explain how P_i and blebbistatin inhibit both actin-activated ATPase and *in vitro* motility to a similar degree. Our results suggest the ADP release rate constant (Fig. 4 and Table 4) plays a significant role in altering the Mg^{2+}-induced changes in actin sliding velocity, whereas changes in actin attachment may also contribute.

Relationship between Strain Sensitivity and Mg^{2+}—The impact of external load or strain on the ADP release step in myosins is well established (60–63). Therefore, it is interesting to propose that that Mg^{2+} sensitivity may have an impact on the load sensing properties of myosins. The structural mechanism of strain sensitivity is unknown, although the conformation of the force-sensing lever arm may be allosterically coupled to structural changes in the nucleotide binding pocket that are associated with ADP binding. The coordination of Mg^{2+} in the

active site may be part of this allosteric coupling pathway. The switch II region has been proposed to play a role in communications between the active site and the lever arm (64). Our previous results that examined mutations in the switch II region of myosin V (55) and the current results demonstrating the Mg^{2+}-induced fluorescence changes in DdMII Trp-501 suggest Mg^{2+} coordination by switch II may be an important part of this mechanism. Further investigation is necessary to elucidate the structural details of the strain-sensitive ADP release mechanism and the role of Mg^{2+} in this process.

Impact on Muscle Function—The cardiac skinned muscle fiber studies clearly demonstrate that attachment time is increased at higher Mg^{2+} concentrations. Thus, in the context of an actively contracting muscle fiber, it is likely that higher Mg^{2+} concentrations slow the ADP release rate constant and reduce contractile velocity. Our results exhibiting unchanged muscle tension as a function of Mg^{2+} support a mechanism by which the rate of attachment is also altered by Mg^{2+}. We propose the rate of attachment and detachment are both altered in the muscle fiber studies, which leads to little change in muscle tension. We would speculate that the overall effect of a reduced detachment rate and preserved tension with increasing Mg^{2+} on muscle performance would include a reduction in maximum contractile power (tension $\times$ velocity) in proportion to the reduction in maximum velocity. The optimum velocity, *i.e.* the velocity at which maximum power is produced, would be also significantly reduced, but the optimum tension would not change. Because the lifetime of the actomyosin·ADP state is load-dependent in both muscle (60) and nonmuscle myosins (61, 63), Mg^{2+} inhibition of contractile velocity may be more pronounced at high loads. The sensitivity of these and other attributes of muscle performance to free Mg^{2+} warrant further investigation.

Our previous work demonstrated a correlation in the actin-activated ATPase activity and *in vitro* motility in four different myosins (MV, SKII, SMII, and NMIIA) (24). A similar relationship was revealed in a landmark study by Barany (65) in that the contractile velocity correlated well with maximal ATPase rate in myosins isolated from a variety of muscles. However, as pointed out by White and co-workers (47), a correlation between actin-activated ATPase rate and sliding velocity does not confirm that the two parameters have the same rate-limiting step. Indeed, experimental results suggest that contractile velocity is limited by detachment from actin, which agrees well with the ADP release rate constant (24, 47), although the ATPase rate is limited by binding to actin and/or phosphate release and is too slow to limit sliding velocity. Our results highlight that Mg^{2+} and temperature can both alter multiple steps in the ATPase cycle, which results in specific changes in contractile velocity and force generation.

We cannot rule out the possibility that Mg^{2+} alters the function of regulatory proteins in muscle, such as troponin C, and the regulatory light chain by competing with calcium-binding sites. One study has addressed this question by examining the Mg^{2+} dependence of rat cardiac muscle with and without hyperthyroid treatment, which shifts the myosin isoform expression in the ventricles from α- to β-cardiac myosin (46). Because the Mg^{2+} dependence of cardiac muscle was more dramatic when α-cardiac myosin was expressed, without a change in myosin light chain expression, they concluded that the impact of Mg^{2+} was associated with its effects on the myosin motor.

Changes in free Mg^{2+} or ADP concentrations will shift the MgADP/ADP ratio causing an impact on myosin motor activity that is limited by the ADP release rate constant (*e.g.* contractile speed and/or intracellular transport). There have been reports that the free Mg^{2+} concentrations in cardiac muscle increase in ischemic heart muscle and thus could play a role in the pathophysiology of heart function (66, 67). Because ischemic episodes are often followed by prolonged hypercontraction without effective relaxation, the Mg^{2+}-induced increase in the myosin cross-bridge lifetime may play a role in this and other pathological conditions. The free Mg^{2+} concentrations increase in skeletal muscle during exercise and initial recovery (68), which suggests that Mg^{2+} could play a role in muscle fatigue. Mg^{2+} concentrations in the brain were found to vary in different neurological disorders (69) and thus could alter the function of myosin motors, such as myosin V, in neurons. A transient influx of Mg^{2+} was found to play a critical role in T-cell activation, and a mutation in the Mg^{2+} transporter associated with this process results in immunodeficiency disease (70). Further studies are necessary to establish the impact of Mg^{2+} in mediating *in vivo* myosin motor function in different pathological and physiological conditions.

Conclusions and Future Directions—We have found that Mg^{2+} alters myosin motor activity by altering steps associated with actin attachment and detachment. The mechanism of altering detachment is likely due to Mg^{2+} exchange in the active site, although it is unclear how Mg^{2+} impacts attachment. Future studies will examine how Mg^{2+} can alter the physiological function of muscle and nonmuscle myosins.

Acknowledgments—We thank William C. Unrath and Matthew Turner for outstanding technical assistance.

REFERENCES

1. Bagshaw, C. R., Eccleston, J. F., Eckstein, F., Goody, R. S., Gutfreund, H., and Trentham, D. R. (1974) The magnesium ion-dependent adenosine triphosphatase of myosin. Two-step processes of adenosine triphosphate association and adenosine diphosphate dissociation. *Biochem. J.* **141,** 351–364
2. Bagshaw, C. R., and Trentham, D. R. (1974) The characterization of myosin-product complexes and of product-release steps during the magnesium ion-dependent adenosine triphosphatase reaction. *Biochem. J.* **141,** 331–349
3. Kintses, B., Gyimesi, M., Pearson, D. S., Geeves, M. A., Zeng, W., Bagshaw, C. R., and Málnási-Csizmadia, A. (2007) Reversible movement of switch 1 loop of myosin determines actin interaction. *EMBO J.* **26,** 265–274
4. Fujita-Becker, S., Dürrwang, U., Erent, M., Clark, R. J., Geeves, M. A., and Manstein, D. J. (2005) Changes in Mg^{2+} ion concentration and heavy chain phosphorylation regulate the motor activity of a class I myosin. *J. Biol. Chem.* **280,** 6064–6071
5. Hannemann, D. E., Cao, W., Olivares, A. O., Robblee, J. P., and De La Cruz, E. M. (2005) Magnesium, ADP, and actin binding linkage of myosin V: evidence for multiple myosin V-ADP and actomyosin V-ADP states. *Biochemistry* **44,** 8826–8840
6. Rosenfeld, S. S., Houdusse, A., and Sweeney, H. L. (2005) Magnesium regulates ADP dissociation from myosin V. *J. Biol. Chem.* **280,** 6072–6079

7. Heissler, S. M., and Manstein, D. J. (2012) Functional characterization of the human myosin-7a motor domain. *Cell. Mol. Life Sci.* **69,** 299–311
8. Vale, R. D. (1996) Switches, latches, and amplifiers: common themes of G proteins and molecular motors. *J. Cell Biol.* **135,** 291–302
9. Trivedi, D. V., Muretta, J. M., Swenson, A. M., Thomas, D. D., and Yengo, C. M. (2013) Magnesium impacts myosin V motor activity by altering key conformational changes in the mechanochemical cycle. *Biochemistry* **52,** 4710–4722
10. De La Cruz, E. M., Wells, A. L., Rosenfeld, S. S., Ostap, E. M., and Sweeney, H. L. (1999) The kinetic mechanism of myosin V. *Proc. Natl. Acad. Sci. U.S.A.* **96,** 13726–13731
11. Olivares, A. O., and De La Cruz, E. M. (2005) Holding the reins on myosin V. *Proc. Natl. Acad. Sci. U.S.A.* **102,** 13719–13720
12. Uemura, S., Higuchi, H., Olivares, A. O., De La Cruz, E. M., and Ishiwata, S. (2004) Mechanochemical coupling of two substeps in a single myosin V motor. *Nat. Struct. Mol. Biol.* **11,** 877–883
13. Chizhov, I., Hartmann, F. K., Hundt, N., and Tsiavaliaris, G. (2013) Global fit analysis of myosin-5b motility reveals thermodynamics of Mg^{2+}-sensitive acto-myosin-ADP states. *PloS One* **8,** e64797
14. Huxley, H. E. (1990) Sliding filaments and molecular motile systems. *J. Biol. Chem.* **265,** 8347–8350
15. Romani, A. M. (2011) Cellular magnesium homeostasis. *Arch. Biochem. Biophys.* **512,** 1–23
16. Buri, A., Chen, S., Fry, C. H., Illner, H., Kickenweiz, E., McGuigan, J. A., Noble, D., Powell, T., and Twist, V. W. (1993) The regulation of intracellular Mg^{2+} in guinea-pig heart, studied with Mg^{2+}-selective microelectrodes and fluorochromes. *Exp. Physiol.* **78,** 221–233
17. Blatter, L. A. (1990) Intracellular free magnesium in frog skeletal muscle studied with a new type of magnesium-selective microelectrode: interactions between magnesium and sodium in the regulation of $[Mg]_i$. *Pflugers Arch.* **416,** 238–246
18. Günzel, D., and Galler, S. (1991) Intracellular free Mg^{2+} concentration in skeletal muscle fibres of frog and crayfish. *Pflugers Arch.* **417,** 446–453
19. Sanders, G. T., Huijgen, H. J., and Sanders, R. (1999) Magnesium in disease: a review with special emphasis on the serum ionized magnesium. *Clin. Chem. Lab. Med.* **37,** 1011–1033
20. Irving, M., Maylie, J., Sizto, N. L., and Chandler, W. K. (1989) Simultaneous monitoring of changes in magnesium and calcium concentrations in frog cut twitch fibers containing antipyrylazo III. *J. Gen. Physiol.* **93,** 585–608
21. Zeng, W., Conibear, P. B., Dickens, J. L., Cowie, R. A., Wakelin, S., Málnási-Csizmadia, A., and Bagshaw, C. R. (2004) Dynamics of actomyosin interactions in relation to the cross-bridge cycle. *Philos. Trans. R. Soc. Lond. B Biol. Sci.* **359,** 1843–1855
22. Nagy, N. T., Sakamoto, T., Takács, B., Gyimesi, M., Hazai, E., Bikádi, Z., Sellers, J. R., and Kovács, M. (2010) Functional adaptation of the switch-2 nucleotide sensor enables rapid processive translocation by myosin-5. *FASEB J.* **24,** 4480–4490
23. De La Cruz, E. M., and Ostap, E. M. (2004) Relating biochemistry and function in the myosin superfamily. *Curr. Opin. Cell Biol.* **16,** 61–67
24. Yengo, C. M., Takagi, Y., and Sellers, J. R. (2012) Temperature-dependent measurements reveal similarities between muscle and nonmuscle myosin motility. *J. Muscle Res. Cell Motil.* **33,** 385–394
25. Sun, M., Oakes, J. L., Ananthanarayanan, S. K., Hawley, K. H., Tsien, R. Y., Adams, S. R., and Yengo, C. M. (2006) Dynamics of the upper 50-kDa domain of myosin V examined with fluorescence resonance energy transfer. *J. Biol. Chem.* **281,** 5711–5717
26. Sweeney, H. L., Rosenfeld, S. S., Brown, F., Faust, L., Smith, J., Xing, J., Stein, L. A., and Sellers, J. R. (1998) Kinetic tuning of myosin via a flexible loop adjacent to the nucleotide binding pocket. *J. Biol. Chem.* **273,** 6262–6270
27. Kovács, M., Thirumurugan, K., Knight, P. J., and Sellers, J. R. (2007) Load-dependent mechanism of nonmuscle myosin 2. *Proc. Natl. Acad. Sci. U.S.A.* **104,** 9994–9999
28. Málnási-Csizmadia, A., Woolley, R. J., and Bagshaw, C. R. (2000) Resolution of conformational states of *Dictyostelium* myosin II motor domain using tryptophan (W501) mutants: implications for the open-closed transition identified by crystallography. *Biochemistry* **39,** 16135–16146
29. Margossian, S. S., and Lowey, S. (1982) Preparation of myosin and its subfragments from rabbit skeletal muscle. *Methods Enzymol.* **85,** 55–71
30. Malmqvist, U. P., Aronshtam, A., and Lowey, S. (2004) Cardiac myosin isoforms from different species have unique enzymatic and mechanical properties. *Biochemistry* **43,** 15058–15065
31. Putkey, J. A., Donnelly, P. V., and Means, A. R. (1987) Bacterial expression vectors for calmodulin. *Methods Enzymol.* **139,** 303–317
32. Pardee, J. D., and Spudich, J. A. (1982) Purification of muscle actin. *Methods Enzymol.* **85,** 164–181
33. Pollard, T. D. (1984) Polymerization of ADP-actin. *J. Cell Biol.* **99,** 769–777
34. Jacobs, D. J., Trivedi, D., David, C., and Yengo, C. M. (2011) Kinetics and thermodynamics of the rate-limiting conformational change in the acto-myosin V mechanochemical cycle. *J. Mol. Biol.* **407,** 716–730
35. De La Cruz, E. M., Sweeney, H. L., and Ostap, E. M. (2000) ADP inhibition of myosin V ATPase activity. *Biophys. J.* **79,** 1524–1529
36. Kron, S. J., Toyoshima, Y. Y., Uyeda, T. Q., and Spudich, J. A. (1991) Assays for actin sliding movement over myosin-coated surfaces. *Methods Enzymol.* **196,** 399–416
37. Meijering, E., Dzyubachyk, O., and Smal, I. (2012) Methods for cell and particle tracking. *Methods Enzymol.* **504,** 183–200
38. Stewart, T. J., Jackson, D. R., Jr., Smith, R. D., Shannon, S. F., Cremo, C. R., and Baker, J. E. (2013) Actin sliding velocities are influenced by the driving forces of actin-myosin binding. *Cell. Mol. Bioeng.* **6,** 26–37
39. Wang, Y., Tanner, B. C., Lombardo, A. T., Tremble, S. M., Maughan, D. W., Vanburen, P., Lewinter, M. M., Robbins, J., and Palmer, B. M. (2013) Cardiac myosin isoforms exhibit differential rates of MgADP release and MgATP binding detected by myocardial viscoelasticity. *J. Mol. Cell. Cardiol.* **54,** 1–8
40. Godt, R. E., and Lindley, B. D. (1982) Influence of temperature upon contractile activation and isometric force production in mechanically skinned muscle fibers of the frog. *J. Gen. Physiol.* **80,** 279–297
41. Bloemink, M. J., Adamek, N., Reggiani, C., and Geeves, M. A. (2007) Kinetic analysis of the slow skeletal myosin MHC-1 isoform from bovine masseter muscle. *J. Mol. Biol.* **373,** 1184–1197
42. Deacon, J. C., Bloemink, M. J., Rezavandi, H., Geeves, M. A., and Leinwand, L. A. (2012) Identification of functional differences between recombinant human α and β cardiac myosin motors. *Cell. Mol. Life Sci.* **69,** 2261–2277
43. Nyitrai, M., Rossi, R., Adamek, N., Pellegrino, M. A., Bottinelli, R., and Geeves, M. A. (2006) What limits the velocity of fast-skeletal muscle contraction in mammals? *J. Mol. Biol.* **355,** 432–442
44. Málnási-Csizmadia, A., and Kovács, M. (2010) Emerging complex pathways of the actomyosin powerstroke. *Trends Biochem. Sci.* **35,** 684–690
45. Yengo, C. M., and Sweeney, H. L. (2004) Functional role of loop 2 in myosin V. *Biochemistry* **43,** 2605–2612
46. Puchert, E., Andruchov, O., Wagner, A., Grassberger, H., Lahnsteiner, F., Sobieszek, A., and Galler, S. (2003) Slowing effects of Mg^{2+} on contractile kinetics of skinned preparations of rat hearts depending on myosin heavy chain isoform content. *Pflugers Arch.* **447,** 135–141
47. Siemankowski, R. F., Wiseman, M. O., and White, H. D. (1985) ADP dissociation from actomyosin subfragment 1 is sufficiently slow to limit the unloaded shortening velocity in vertebrate muscle. *Proc. Natl. Acad. Sci. U.S.A.* **82,** 658–662
48. Moore, J. R., Krementsova, E. B., Trybus, K. M., and Warshaw, D. M. (2004) Does the myosin V neck region act as a lever? *J. Muscle Res. Cell Motil.* **25,** 29–35
49. Tyska, M. J., Dupuis, D. E., Guilford, W. H., Patlak, J. B., Waller, G. S., Trybus, K. M., Warshaw, D. M., and Lowey, S. (1999) Two heads of myosin are better than one for generating force and motion. *Proc. Natl. Acad. Sci. U.S.A.* **96,** 4402–4407
50. Lauzon, A. M., Tyska, M. J., Rovner, A. S., Freyzon, Y., Warshaw, D. M., and Trybus, K. M. (1998) A 7-amino-acid insert in the heavy chain nucleotide binding loop alters the kinetics of smooth muscle myosin in the laser trap. *J. Muscle Res. Cell Motil.* **19,** 825–837
51. Nagy, A., Takagi, Y., Billington, N., Sun, S. A., Hong, D. K., Homsher, E., Wang, A., and Sellers, J. R. (2013) Kinetic characterization of nonmuscle myosin IIb at the single molecule level. *J. Biol. Chem.* **288,** 709–722

52. Tyska, M. J., Hayes, E., Giewat, M., Seidman, C. E., Seidman, J. G., and Warshaw, D. M. (2000) Single-molecule mechanics of R403Q cardiac myosin isolated from the mouse model of familial hypertrophic cardiomyopathy. *Circ. Res.* **86,** 737–744
53. Rosenfeld, S. S., and Sweeney, H. L. (2004) A model of myosin V processivity. *J. Biol. Chem.* **279,** 40100–40111
54. Forgacs, E., Cartwright, S., Sakamoto, T., Sellers, J. R., Corrie, J. E., Webb, M. R., and White, H. D. (2008) Kinetics of ADP dissociation from the trail and lead heads of actomyosin V following the power stroke. *J. Biol. Chem.* **283,** 766–773
55. Trivedi, D. V., David, C., Jacobs, D. J., and Yengo, C. M. (2012) Switch II mutants reveal coupling between the nucleotide- and actin-binding regions in myosin V. *Biophys. J.* **102,** 2545–2555
56. Milligan, R. A. (1996) Protein-protein interactions in the rigor actomyosin complex. *Proc. Natl. Acad. Sci. U.S.A.* **93,** 21–26
57. Geeves, M. A., and Conibear, P. B. (1995) The role of three-state docking of myosin S1 with actin in force generation. *Biophys. J.* **68,** 194S-199S
58. Sun, M., Rose, M. B., Ananthanarayanan, S. K., Jacobs, D. J., and Yengo, C. M. (2008) Characterization of the pre-force-generation state in the actomyosin cross-bridge cycle. *Proc. Natl. Acad. Sci. U.S.A.* **105,** 8631–8636
59. Jackson, D. R., Jr., Webb, M., Stewart, T. J., Phillips, T., Carter, M., Cremo, C. R., and Baker, J. E. (2014) Sucrose increases the activation energy barrier for actin-myosin strong binding. *Arch. Biochem. Biophys.* **552–553,** 74–82
60. Nyitrai, M., and Geeves, M. A. (2004) Adenosine diphosphate and strain sensitivity in myosin motors. *Philos. Trans. R. Soc. Lond. B Biol. Sci.* **359,** 1867–1877
61. Laakso, J. M., Lewis, J. H., Shuman, H., and Ostap, E. M. (2008) Myosin I can act as a molecular force sensor. *Science* **321,** 133–136
62. Sellers, J. R., and Veigel, C. (2010) Direct observation of the myosin-Va power stroke and its reversal. *Nat. Struct. Mol. Biol.* **17,** 590–595
63. Oguchi, Y., Mikhailenko, S. V., Ohki, T., Olivares, A. O., De La Cruz, E. M., and Ishiwata, S. (2008) Load-dependent ADP binding to myosins V and VI: implications for subunit coordination and function. *Proc. Natl. Acad. Sci. U.S.A.* **105,** 7714–7719
64. Geeves, M. A., and Holmes, K. C. (1999) Structural mechanism of muscle contraction. *Annu. Rev. Biochem.* **68,** 687–728
65. Bárány, M. (1967) ATPase activity of myosin correlated with speed of muscle shortening. *J. Gen. Physiol.* **50,** 197–218
66. Headrick, J. P., and Willis, R. J. (1991) Cytosolic free magnesium in stimulated, hypoxic, and underperfused rat heart. *J. Mol. Cell. Cardiol.* **23,** 991–999
67. Murphy, E., Steenbergen, C., Levy, L. A., Raju, B., and London, R. E. (1989) Cytosolic free magnesium levels in ischemic rat heart. *J. Biol. Chem.* **264,** 5622–5627
68. Iotti, S., Frassineti, C., Alderighi, L., Sabatini, A., Vacca, A., and Barbiroli, B. (2000) *In vivo* ^{31}P-MRS assessment of cytosolic [Mg^{2+}] in the human skeletal muscle in different metabolic conditions. *Magn. Reson. Imaging* **18,** 607–614
69. Iotti, S., and Malucelli, E. (2008) *In vivo* assessment of Mg^{2+} in human brain and skeletal muscle by ^{31}P-MRS. *Magnes. Res.* **21,** 157–162
70. Li, F. Y., Chaigne-Delalande, B., Kanellopoulou, C., Davis, J. C., Matthews, H. F., Douek, D. C., Cohen, J. I., Uzel, G., Su, H. C., and Lenardo, M. J. (2011) Second messenger role for Mg^{2+} revealed by human T-cell immunodeficiency. *Nature* **475,** 471–476
71. Cahours, X., Morin, P. H., and Dreux, M. (1998) Capillary electrophoretic study of the complexation of nucleotides with magnesium and calcium ions. *Chromatographia* **48,** 739–744